SCIENCE CHINA
Information Sciences

• RESEARCH PAPER •

December 2020, Vol. 63 222401:1–222401:9
https://doi.org/10.1007/s11432-020-3058-2

Narrow bandwidth fiber-optic spectral combs for renewable hydrogen detection

Shunshuo CAI[1†], Fu LIU[2†], Runlin WANG[1], Yongguang XIAO[1], Kaiwei LI[1], Christophe CAUCHETEUR[3] & Tuan GUO[1*]

[1]*Institute of Photonics Technology, Jinan University, Guangzhou* 510632*, China;*
[2]*Department of Electronics, Carleton University, Ottawa* K1S 5B6*, Canada;*
[3]*Electromagnetism and Telecommunications Department, University of Mons, Mons* 7000*, Belgium*

Received 21 May 2020/Revised 27 July 2020/Accepted 3 September 2020/Published online 12 November 2020

Abstract Hydrogen sensors are of great importance to detect leakage in time because the hydrogen-air mixture is highly flammable. Based on optical fiber-based configurations reported so far, using palladium coating only does not meet stringent performance targets, such as fast response time and limited deactivation caused by poisoning. Here, a palladium-gold alloy-coated optical fiber hydrogen sensor, i.e., highly tilted fiber Bragg grating (TFBG), was proposed by using its narrow bandwidth cladding modes whose effective refractive index (ERI) extends to 1.0 where the gas measurement is possible, which led to faster specific hydrogen measurement response time (a shorter stabilization time during the association and dissociation phases less than 20 s and 30 s, respectively) and improved deactivation resistance (higher than 99% per test cycle). Meanwhile, the temperature cross-sensitivity can be eliminated via referencing the "target" spectral combs to the core mode. We are sure that this promising configuration extends research directions for rapid, repeatable and high deactivation-resistance in hydrogen gas detection.

Keywords fiber-optic sensing probe, tilted fiber Bragg grating, hydrogen measurement, palladium-gold alloy nanocoating

Citation Cai S S, Liu F, Wang R L, et al. Narrow bandwidth fiber-optic spectral combs for renewable hydrogen detection. Sci China Inf Sci, 2020, 63(12): 222401, https://doi.org/10.1007/s11432-020-3058-2

1 Introduction

Considering as one of the promising candidates for renewable alternatives [1], hydrogen is acting as a clean energy carrier taking merits of high energy-density, carbon-free, and pollution-free [2–4]. However, any leaks in hydrogen must be detected immediately for all related systems due to safety reasons (highly flammable for hydrogen-air mixture). In contrast with other method solving these challenging targets, the hydrogen sensors using optical fiber-based configuration have been widely investigated [5, 6], which are attractive for its inherent features such as corrosion resistance, immunity to electromagnetic waves (or radiation), and the ability to work remotely [7–11]. The key point is that the optical signal generates no sparks during sensing, comparing to that of the electrical signal. Mostly, the highly hydrogen-selective metal is integrated into the sensing system by absorbing the hydrogen molecule into interstitials of metal host and in turn modulates the sensing signal [12]. In this field, palladium (Pd) is one of the most popular and widely used functional materials for specific hydrogen detection [13–17] because the reversible phase transition from metal to metal hydride after capturing hydrogen molecule is happening

* Corresponding author (email: tuanguo@jnu.edu.cn)
† Cai S S and Liu F have the same contribution to this work.

© Science China Press and Springer-Verlag GmbH Germany, part of Springer Nature 2020

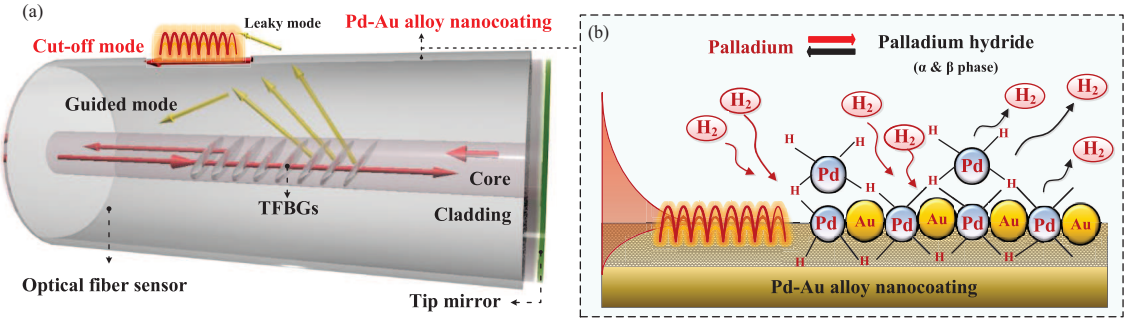

Figure 1 (Color online) (a) The schematic of TFBG in terms of cut-off surface resonance hydrogen sensing principle; (b) the sketch of hydrogen-induced phase transition from metal state to metal hydride state over palladium-gold alloy nanocoating.

at room temperature [18], which consequently modifies its optical dielectric constant [19–21]. A widely encountered problem is that some natural gases in the air, even at ppm concentrations, can poison the hydrogen dissociation and diffusion into the Pd crystal lattice [22–24]. This poisoning of the Pd results in several drawbacks, such as hysteretic behavior, longer response time and deactivation of the Pd [25]. In addition, environmental changes (such as humidity and temperature variations) will also induce unpredictable inaccuracy in the measurement results [26, 27].

Based on the limitation discussed above, we proposed a palladium-gold-alloy coated optical fiber sensing configuration using tilted fiber Bragg grating (TFBG) inscribed in single-mode fiber which couples the core mode (forward propagation) to larger numbers of discrete cladding modes (backward propagation) [28–31] whose evanescent field can go through the coated layer for sensing or achieving other physics phenomena such as surface plasmon polaritons excitation by interacting with a conductive metal layer [32–35]. In contrast to TFBG working in liquid environment, a highly tilted TFBG (corresponding tilted angle larger than 35°) does the favor to couple the core mode to higher-order cladding modes with an effective refractive index (ERI) close to 1.0, making them suitable for gas-phase measurement. Meanwhile, it provides a self-calibration ability to alleviate the temperature cross-sensitivity by referencing the wavelength of cladding mode resonance to core mode which is insensitive to external refractive index perturbation [28, 29]. By using a palladium-gold alloy nanocoating (rather than pure palladium coating as previously reported), we have achieved a shorter stabilization time during the association and dissociation phases (less than 20 s and 30 s, respectively) and improved deactivation resistance (higher than 99% per test cycle) for *in situ* hydrogen measurement, which demonstrates its potential as a promising method for rapid, repeatable, and highly effective resistance to deactivation of hydrogen gas detection.

2 Materials and methods

2.1 Fabrication of TFBG

The schematic of TFBG shown in Figure 1(a), a 16-mm long TFBG was manufactured in standard telecom single-mode fiber based on the phase-mask method well described in [28, 29]. The high tilted angle up to 37° (external tilt angle between the incident laser and fiber normal direction) was achieved via rotating the fiber and phase mask together following the direction perpendicular to fiber orientation, thus the cladding modes with an ERI near 1.0 could be excited, so-called cut-off cladding mode in air, for gaseous measurement.

2.2 Pd-Au alloy nanocoating

The Pd-Au alloy nanocoating was deposited on the surface of fiber via magnetron sputtering. To enable higher-quality nanocoating film three steps are considered. Firstly, a chromium layer with a 3-nm thick was sandwiched between the fiber and Pd-Au alloy nanocoating to improve the adhesion strength of the

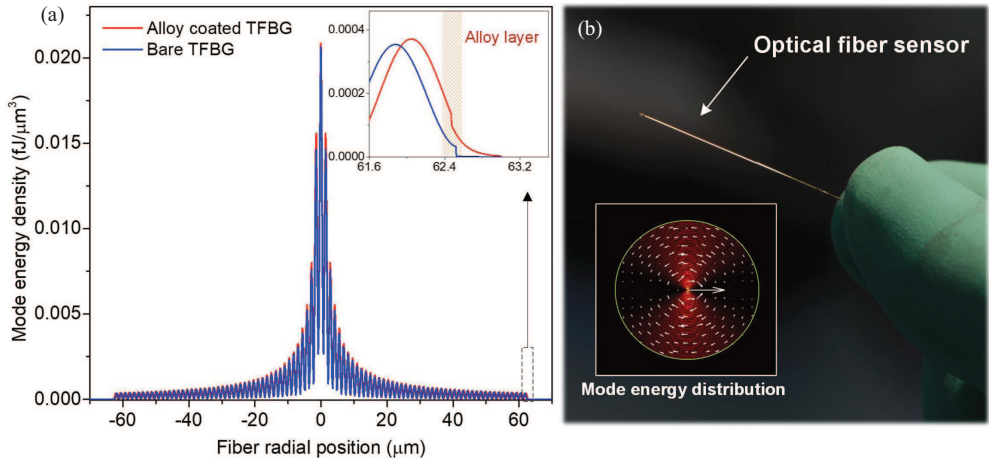

Figure 2 (Color online) (a) Simulation of the cut-off mode's energy distribution when TFBG with and without Pd-Au alloy coating in S-polarized light. The inlay highlight enlarged detail of the energy distribution on the surface of the alloy layer. (b) Photograph of the Pd-Au alloy coated fiber-optic sensor. Inset: cross-section of the cut-off mode's energy distribution.

target coating layer. Secondly, Pd and Au targets are simultaneously sputtered using a single common radio-frequency (RF) power source to make sure the two species are uniformly mixed. The deposition condition here, e.g., pressure is 1E−3 Pa, RF power is 125 W. Finally, to achieve more uniform coating around the cladding surface, the optical fiber rotates around its axis at a constant speed of 0.5 rad/s. Therefore, the uniformity of Pd-Au alloy nanocoating onto the fiber could be achieved, which strongly improve the sensing performance and underpin the resonance visibility [36]. The concentration of 56% Au, and a thickness of 50 nm has been successfully coated on the surface of TFBGs.

2.3 Sensing methods

The simulations computed the cut-off cladding azimuthally polarized modes, obtaining the results shown in Figure 2(a) for TFBG with and without Pd-Au alloy nanocoating, respectively. The simulation parameters were a core radius of 4.5 μm with a refractive index of 1.4545 RIU (refractive index unit), a cladding radius of 62.5 μm with a refractive index of 1.4467 RIU. The Pd-Au alloy nanocoating was with the thickness of 50 nm with a complex refractive index of $1.8104 + 8.7381i$, which calculated according to the Lorentz-Lorenz equation [37,38]: $(n_{12}^2 - 1)/(n_{12}^2 + 2) = \varphi_1(n_1^2 - 1)/(n_1^2 + 2) + \varphi_2(n_2^2 - 1)/(n_2^2 + 2)$, where n_{12} is the refractive index of the Pd-Au alloy, n_1 and n_2 are the indexes of Au $(0.41915 + 9.3327i)$ and Pd $(2.7810 + 7.5483i)$ [39], respectively, and φ_1 and φ_2 are the volume fractions of the two components. Validating simulation results can be plotted as the mode energy density against the fiber radial position. As can be seen, the mode energy distribution on the surface of the layer of Pd-Au alloy coated TFBG is stronger than bare TFBG. This energy increase leads to a greater resonance of the corresponding cladding mode whose evanescent field extends furthest from the cladding and consequently exhibits the increasing sensitivity to surrounding refractive index (SRI) [40]. Figure 2(b) shows the configuration of Pd-Au alloy coated tilted fiber Bragg grating sensor. The inset shows the mode energy distribution of the cut-off mode resonance of the Pd-Au alloy coated TFBG over the fiber's cross-section.

It is well known that the TFBG structure can couple the incident core mode into the reflected core mode and a large number of reflected cladding modes. The guided cladding modes have an ERI higher than an SRI, and are thus totally internally reflected inside the fiber, while the leaky cladding modes, whose ERI is less than the SRI, will be cut off [41]. The cut-off mode resonance shown by the red asterisk marked on the black curve of Figure 3, is the mode whose evanescent field extends furthest from the cladding and consequently exhibits the maximum sensitivity to SRI. The boundary, also called cut-off condition [42], has the characteristic of a sharply reduced amplitude of the resonance owing to a sudden increase of mode loss. It is worth noting that the maximum of the resonance amplitudes shifts toward the lower wavelengths when the tilt angle is increasing, thus the cut-off wavelength shifts as well. In this

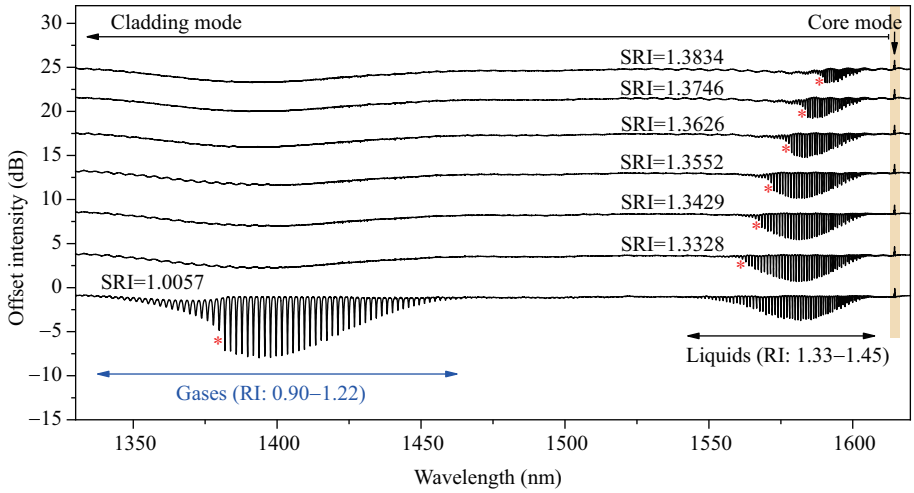

Figure 3 (Color online) Transmission spectra of bare 37° TFBG as a function of SRI (offset on the vertical scale, and the cut-off position is marked by the red asterisk).

work, we track a cut-off surface resonance. Instead of other fiber-optic based hydrogen sensors whose principle is the swelling of a Pd film as it becomes loaded with hydrogen [43], in our work we exploit the optical response of this sensor as the metal coating converts from Pd to Pd hydride in the presence of hydrogen gas. Also, the higher α-phase solubility and the deformation suppressed of the Pd-Au alloy can be achieved during the hydrogen-induced phase transition. This scheme offers outstanding sensing characteristics for rapid hydrogen detection and is highly resistant to deactivation. The optical response is much faster than the swelling and can be properly measured by our sensing platform.

Figure 3 shows the transmission spectra of a 37° TFBG, in which the internal tilt angle was 23°, and this angle difference is original from the RI difference between the fiber cladding (∼1.445) and outside air (∼1.002). The numerous cladding modes extending from 1350 to 1600 nm can be divided into two main subsets: one group of cladding modes, in the wavelength ranging from 1530 to 1612 nm, has effective refractive indices range of 1.33–1.45. Consequently, this group of cladding modes is suitable for measurement in water solutions. Another group of cladding modes, in the wavelength ranging from 1320 to 1460 nm, has effective refractive indices range of 0.90–1.22, constitutes the key elements of cladding modes with a phase-matching condition to the air and the specific gas to be measured.

3 Results and discussion

3.1 Experimental setup

The performance of the sensor for hydrogen detection was evaluated by introducing the optical fiber probe into a gas chamber and using the setup illustrated in Figure 4. A broadband light source (BBS, Golight OS-EB-LD-1450-400-30-S-FA, working range from 1230 to 1680 nm, spectral density is −25 dBm/nm) was connected to a polarization controller to ensure the input is linearly polarized for S- or P- polarization relative to the grating plane, and finally the output was detected by a optical spectrum analyzer (OSA, Yokogawa AQ6370D). Two gas inlets, i.e., hydrogen (H_2) and air, are incorporated into the gas chamber. Hence, different H_2 concentrations can be achieved with rapid concentration switching by adjusting the flow difference between the two gases.

3.2 Improved sensing characteristics

Figure 5 depicts the transmitted optical spectra of a 37° TFBG with and without Pd-Au alloy coating surrounded by air. The red asterisk placed in the blue curve of Figure 5(a) indicates the position of the cut-off mode in air, corresponding to the cladding mode for which the ERI matches the SRI of the gas

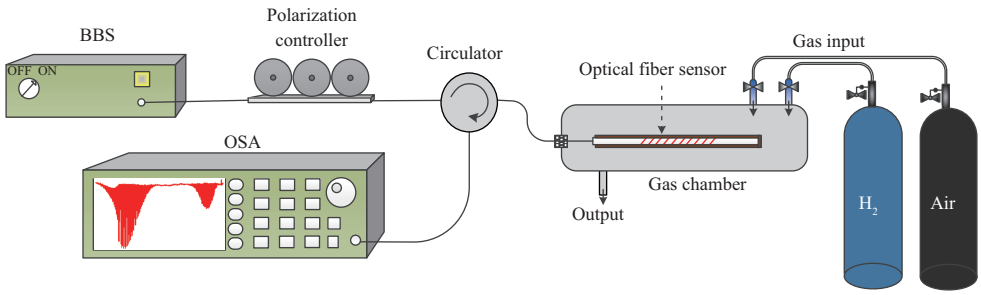

Figure 4 (Color online) The setup to clarify the sensing characteristics of the sensor in the hydrogen environment.

medium. Cladding modes at the shorter side of the cut-off wavelength come within the class of leaky cladding modes.

When we observe the cut-off resonance (near the red asterisk in Figure 5(a), and in the expanded view in Figure 5(b)) we note a marked change in its amplitude according to whether the surrounding gas is pure air (blue curve in Figure 5(b)) or air with 2% hydrogen gas added (red curve in Figure 5(b)). It should be noted that the expected refractive index difference in the gas should be only at the level of 10^{-6} to 10^{-7} RIU. Therefore, the strong change in amplitude of cut-off resonance must mainly originate from the ERI modulation of the Pd-Au alloy film covering the fiber surface, which is essentially due to the insertion of atomic hydrogen into the Pd crystal lattice and the consequently induced reversible phase transition of Pd-Au alloy from a metal to a metal hydride state, as shown in Figure 1(b). The Bragg resonance – the core mode – at the longest wavelength of 1614.5 nm, as can be seen in Figure 5(c), remains virtually unchanged intensity and unshifted wavelength, confirming that the change of the cut-off mode arises from SRI changes of the gas media and not from physical effects such as temperature or strain. Any undesirable temperature and intensity level fluctuation effects can therefore be subtracted from the sensor response.

Figure 6 depicts the real-time optical response of the fiber-optic sensing probe to hydrogen with two different nanocoatings: pure Pd and Pd-Au alloy, respectively. The H_2 concentration is 2% in air (lower than the explosive concentration of 4%) and is abruptly changed to 0% by introducing airflow. Compared to the pure Pd coating, the stabilization time during the association phase has been greatly reduced from 90 to 20 s by using Pd-Au alloy. Meanwhile, the stabilization time during the dissociation phase has also been decreased from 120 to 30 s. This is because the Pd-Au alloy has a higher α-phase solubility when the absorbed hydrogen occupies the octahedral interstices of the Pd lattice at room temperature [44]. Thus the stabilization times during the association and dissociation phases are faster.

Figure 7 shows a response of hydrogen sensor for detecting repetitive H_2 concentration cycling between 0% and 2% H_2 by volume concentration in air. The relative optical amplitude changes are higher when the fiber sensor coated with pure Pd than with the Pd-Au alloy. However, the signal-noise-ratio of the fiber sensor with pure Pd is lower than that of the Pd-Au alloy coating, due to the stronger fluctuations over the 2% H_2 testing period. More importantly, the repeatability of the sensor for hydrogen cycling detection has been significantly improved by using the Pd-Au alloy nanocoating. As the dash-dot-lines marked in Figure 7, a strong hydrogen deactivation of 7% has been founded in the pure Pd nanocoated sensor while there is less than 1% deactivation in the Pd-Au alloy nanocoating. This is because the surface of the Pd-Au alloy was much more resistant to hydrogen-induced deformation for the above test cycle than pure Pd was.

Figure 8(a) presents the response of the Pd-Au alloy nanocoated sensor to the presence of different concentrations hydrogen. As can be seen, the sensor, that reacts to H_2 concentrations of 0.5%, 1%, 1.5%, and 2% (in volume), exhibits excellent recovery of the baseline. All of those concentrations are below the lower explosive limit of the H_2 concentration of 4%. The linear response with a correlation coefficient of 99% is obtained using our sensor at concentrations in air from 0% to 2% as shown in Figure 8(b). Long time and constant hydrogen concentration detection show that the average standard deviation of

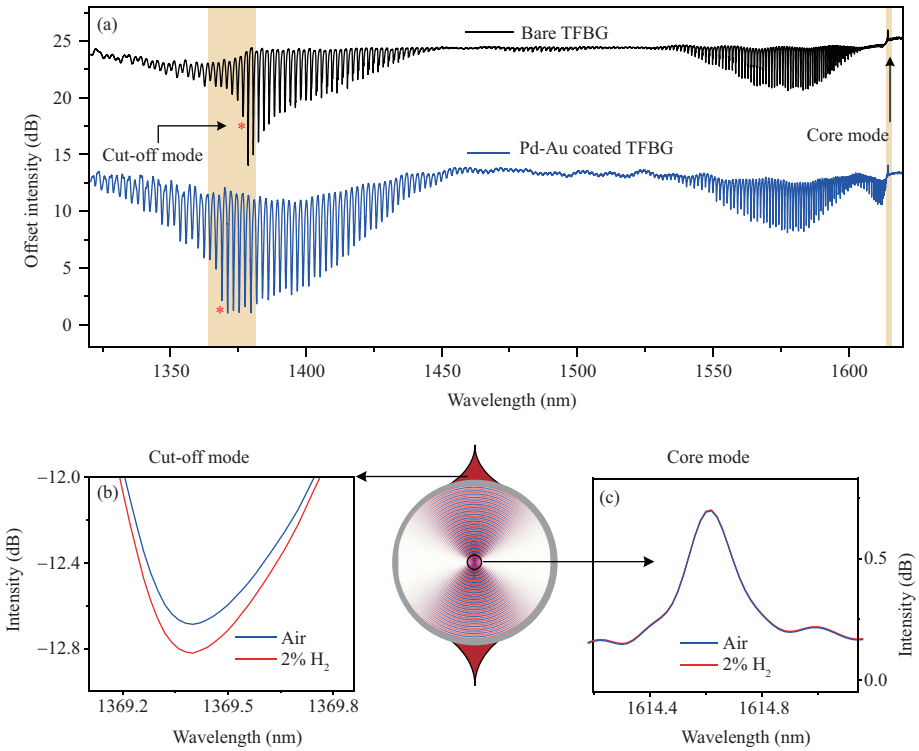

Figure 5 (Color online) (a) The transmitted amplitude spectra of a bare TFBG and Pd-Au alloy nanocoated TFBG in air; (b) the enlarged detail of the cut-off surface mode resonance when a sensor is exposed to pure air to air with 2% hydrogen and a schematic cross-section of cut-off mode's optical field distribution for the Pd-Au alloy nanocoated TFBG; (c) the core mode used as for temperature elimination.

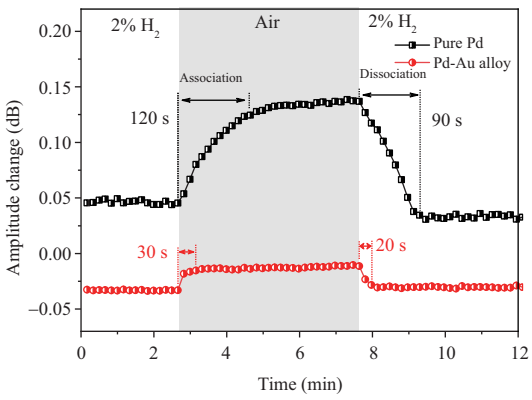

Figure 6 (Color online) Sensor's response time for hydrogen detection with pure Pd and Pd-Au alloy nanocoatings.

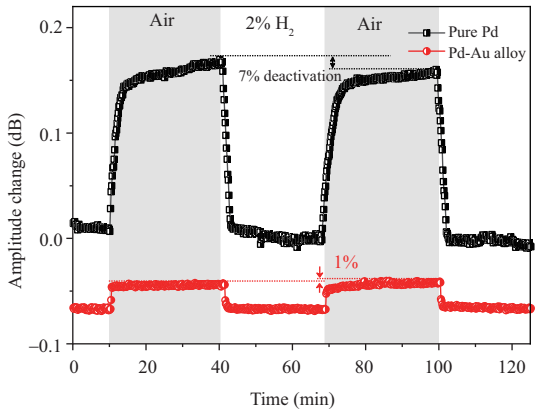

Figure 7 (Color online) Sensor's repeatability in the hydrogen cycling detection with pure Pd and Pd-Au alloy nanocoatings, respectively.

the optical intensity of the cut-off mode was ± 0.002 dB. Thus, the limit of detection (LOD) of our sensor is about 2300 ppm, which limited by the slight fluctuation of the BBS (especially around 1370 nm, where the cut-off mode was monitored). This problem can be definitely solved by using a real-time interrogation scheme based on a power measurement [45]. In this case, tunable laser (TLS) with narrow bandwidth spectral combs, was used as a source, and an analog-to-digital converter obtains the output data from photodiode as a detector instead of OSA. The wavelength of TLS is probed the transmitted power spectrum at the cut-off mode of the TFBG, determined by initial calibration with an OSA. The intensity change results from the mode wavelength shift relative to the fixed wavelength of TLS due to the

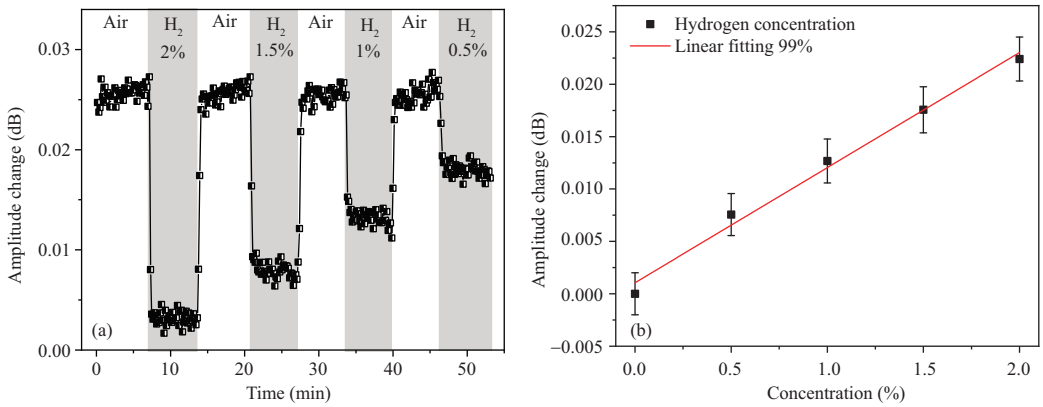

Figure 8 (Color online) (a) Sensing response of hydrogen with the concentration range from 0%–2% in volume; (b) the linear response of the sensor.

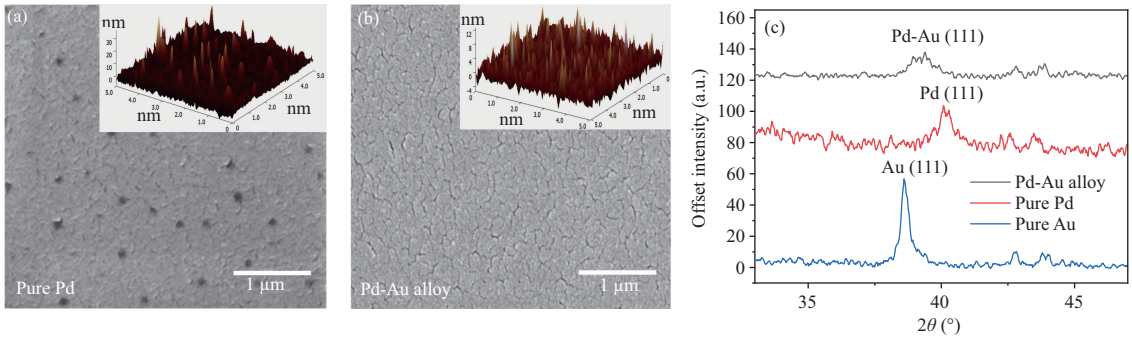

Figure 9 (Color online) Morphology of the nanocoatings (a) pure Pd, (b) Pd-Au alloy after the sensor is exposed to the presence of the hydrogen, and (c) X-ray diffractograms of coating materials over the fiber.

principle of edge filtering. In addition, for the end-users, such a simplified and cost-effective interrogation scheme can be considered to use in the industry.

Both surface morphology of pure Pd and Pd-Au alloy, which have equal thickness before, were examined after hydrogen cycling detection illustrated in Figure 9(a) and (b). The images were obtained using a scanning electron microscope (SEM) and atomic force microscopy (AFM), respectively. There are some cracks in the pure Pd and Pd-Au alloy nanofilms after exposure to the hydrogen environment. Most of those cracks are caused by the process of magnetron sputtering when the Pd-Au alloy or Pd was deposited around the fiber surface. But in the case of pure coating Pd as shown in Figure 9(a), much larger pore structures are seen over the surface after the sensor is exposed to the environment of 2% hydrogen, while the Pd-Au alloy surface shown in Figure 9(b) is smoother with small, dense cracks. As the SEM image in Figure 9(a) shows, the pure Pd hydride is more susceptible to deformation during the process of hydrogen-induced phase transition. This problem could be highly suppressed by using Pd-Au alloy. Representative AFM images of pure Pd and Pd-Au alloy surfaces are shown in the inlay of Figure 9(a) and (b), their roughness (R_a) is 1.713 and 1.559 nm, respectively. Finally, Figure 9(c) presents the X-ray diffractograms of coating materials over the fiber surface using magnetron sputtering. Clearly, three components have been found with peaks corresponding to the monometallic Pd (red curve), the monometallic Au (blue curve), and the bimetallic Pd-Au alloy (black curve), which demonstrated the presence of gold, palladium and the bimetallic Pd-Au alloys.

4 Conclusion

The cut-off surface resonance hydrogen sensing based on palladium-gold alloy nanocoated optical fiber sensor through a 16 mm in length, 37°-tilted TFBG (i.e., the excited narrowband cladding mode combs

cover the refractive index region of gas measurement near 1.0) has been proposed and experimentally demonstrated, resulting from its largest evanescent field exhibiting the maximum sensitivity to permittivity perturbation of coated layer. The faster response time (a stabilization time during the association and dissociation phases are less than 20 and 30 s, respectively) and improved deactivation resistance have been achieved for specific hydrogen measurement by detecting the strength of cut-off mode resonance. This all-optical configuration opens a research direction for rapid, repeatable and highly effective resistance to deactivation of hydrogen gas. It is promising to be further used under harsh conditions, like the implantation of the sensor into a hydrogen-fuel cell for *in situ* renewable energy vehicle monitoring [46].

Acknowledgements This work was supported by National Natural Science Foundation of China (Grant Nos. 62035006, 61722505, 61975068, 62005101), Key Program of the Guangdong Natural Science Foundation (Grant No. 2018B030311006), Guangdong Outstanding Scientific Innovation Foundation (Grant No. 2019TX05X383), Program of the China Scholarship Council (Grant No. 201806780010), and Fonds de la Recherche Scientifique (FNRS) (Grant No. O001518F).

References

1 She X Y, Shen Y, Wang J F, et al. Pd films on soft substrates: a visual, high-contrast and low-cost optical hydrogen sensor. Light Sci Appl, 2019, 8: 4
2 Xiao M M, Liang S B, Han J, et al. Batch fabrication of ultrasensitive carbon nanotube hydrogen sensors with sub-ppm detection limit. ACS Sens, 2018, 3: 749–756
3 Wang Y, Zhao Z T, Sun Y J, et al. Fabrication and gas sensing properties of Au-loaded SnO_2 composite nanoparticles for highly sensitive hydrogen detection. Sens Actuat B-Chem, 2017, 240: 664–673
4 Zhang Z Y, Zou X M, Xu L, et al. Hydrogen gas sensor based on metal oxide nanoparticles decorated graphene transistor. Nanoscale, 2015, 7: 10078–10084
5 Ma J, Zhou Y L, Bai X, et al. High-sensitivity and fast-response fiber-tip Fabry-Pérot hydrogen sensor with suspended palladium-decorated graphene. Nanoscale, 2019, 11: 15821–15827
6 Fong N R, Berini P, Tait R N. Hydrogen sensing with Pd-coated long-range surface plasmon membrane waveguides. Nanoscale, 2016, 8: 4284–4290
7 Ji Y F, Lu C, Zibar D, et al. Special focus on artificial intelligence for optical communications. Sci China Inf Sci, 2020, 63: 160300
8 Pu G Q, Zhang L, Hu W S, et al. Automatic mode-locking fiber lasers: progress and perspectives. Sci China Inf Sci, 2020, 63: 160404
9 Caucheteur C, Guo T, Liu F, et al. Ultrasensitive plasmonic sensing in air using optical fibre spectral combs. Nat Commun, 2016, 7: 13371
10 Jiao Y Q, Cao Z Z. Photonic integration technologies for indoor optical wireless communications. Sci China Inf Sci, 2018, 61: 080404
11 Ma G M, Li C R, Mu R D, et al. Fiber bragg grating sensor for hydrogen detection in power transformers. IEEE Trans Dielect Electr Insul, 2014, 21: 380–385
12 Nugroho F A A, Darmadi I, Cusinato L, et al. Meta-polymer hybrid nanomaterials for plasmonic ultrafast hydrogen detection. Nat Mater, 2019, 18: 489–495
13 Victoria M, Westerwaal R J, Dam B, et al. Amorphous metal-hydrides for optical hydrogen sensing: the effect of adding glassy Ni-Zr to Mg-Ni-H. ACS Sens, 2016, 1: 222–226
14 Noh J S, Kim H, Kim B S, et al. High-performance vertical hydrogen sensors using Pd-coated rough Si nanowires. J Mater Chem, 2011, 21: 15935
15 Lin K Q, Lu Y H, Chen J X, et al. Surface plasmon resonance hydrogen sensor based on metallic grating with high sensitivity. Opt Express, 2008, 16: 18599–18604
16 Wang Z J, Li Z Y, Jiang T T, et al. Ultrasensitive hydrogen sensor based on Pd^0-loaded SnO_2 electrospun nanofibers at room temperature. ACS Appl Mater Interfaces, 2013, 5: 2013–2021
17 Cho M, Zhu J X, Kim H, et al. Half-pipe palladium nanotube-based hydrogen sensor using a suspended nanofiber scaffold. ACS Appl Mater Interfaces, 2019, 11: 13343–13349
18 Zhang X J, Cai S S, Liu F, et al. In situ determination of the complex permittivity of ultrathin H_2-infused palladium coatings for plasmonic fiber optic sensors in the near infrared. J Mater Chem C, 2018, 6: 5161–5170
19 Masuzawa S, Okazaki S, Maru Y, et al. Catalyst-type-an optical fiber sensor for hydrogen leakage based on fiber Bragg gratings. Sens Actuat B-Chem, 2015, 217: 151–157
20 Caucheteur C, Debliquy M, Lahem D, et al. Catalytic fiber bragg grating sensor for hydrogen leak detection in air. IEEE Photon Technol Lett, 2008, 20: 96–98
21 Wadell C, Syrenova S, Langhammer C. Plasmonic hydrogen sensing with nanostructured metal hydrides. ACS Nano, 2014, 8: 11925–11940
22 Hübert T, Boon-Brett L, Black G, et al. Hydrogen sensors — a review. Sens Actuat B-Chem, 2011, 157: 329–352
23 Palmisano V, Weidner E, Boon-Brett L, et al. Selectivity and resistance to poisons of commercial hydrogen sensors. Int J Hydrogen Energy, 2015, 40: 11740–11747
24 Clerbaux C, Edwards D P, Deeter M, et al. Carbon monoxide pollution from cities and urban areas observed by the

Terra/MOPITT mission. Geophys Res Lett, 2008, 35: 03817
25 Schwarz R B, Khachaturyan A G. Thermodynamics of open two-phase systems with coherent interfaces: application to metal-hydrogen systems. Acta Mater, 2006, 54: 313–323
26 Cai S S, González-Vila, Zhang X J, et al. Palladium-coated plasmonic optical fiber gratings for hydrogen detection. Opt Lett, 2019, 44: 4483–4486
27 Sayago I, Terrado E, Aleixandre M, et al. Novel selective sensors based on carbon nanotube films for hydrogen detection. Sens Actuat B-Chem, 2007, 122: 75–80
28 Albert J, Shao L Y, Caucheteur C. Tilted fiber Bragg grating sensors. Laser Photonics Rev, 2013, 7: 83–108
29 Guo T. Fiber grating-assisted surface plasmon resonance for biochemical and electrochemical sensing. J Lightwave Technol, 2017, 35: 3323–3333
30 Xu O, Lu S H, Jian S S. Theoretical analysis of polarization properties for tilted fiber Bragg gratings. Sci China Inf Sci, 2010, 53: 390–397
31 Lu S H, Xu O, Feng S C, et al. Analysis of coupling from core mode to counter-propagating radiation modes in tilted fiber Bragg gratings. Sci China Inf Sci, 2010, 53: 1078–1088
32 Sypabekova M, Korganbayev S, González-Vila, et al. Functionalized etched tilted fiber Bragg grating aptasensor for label-free protein detection. Biosens Bioelectron, 2019, 146: 111765
33 Si Y, Lao J J, Zhang X J, et al. Electrochemical plasmonic fiber-optic sensors for ultra-sensitive heavy metal detection. J Lightwave Technol, 2019, 37: 3495–3502
34 Marquez-Cruz V, Albert J. High resolution NIR TFBG-assisted biochemical sensors. J Lightwave Technol, 2015, 33: 3363–3373
35 Liu F, Albert J. 40 GHz-rate all-optical cross-modulation of core-guided near infrared light in single mode fiber by surface plasmons on gold-coated tilted fiber Bragg gratings. APL Photonics, 2019, 4: 126104
36 Chiavaioli F, Gouveia C, Jorge P, et al. Towards a uniform metrological assessment of grating-based optical fiber sensors: from refractometers to biosensors. Biosensors, 2017, 7: 23
37 Chen H J, Kou X S, Yang Z, et al. Shape- and size-dependent refractive index sensitivity of gold nanoparticles. Langmuir, 2008, 24: 5233–5237
38 Mehra R. Application of refractive index mixing rules in binary systems of hexadecane and heptadecane withn-alkanols at different temperatures. J Chem Sci, 2003, 115: 147–154
39 Johnson P, Christy R. Optical constants of transition metals: Ti, V, Cr, Mn, Fe, Co, Ni, and Pd. Phys Rev B, 1974, 9: 5056–5070
40 Chiavaioli F, Zubiate P, Del Villar I, et al. Femtomolar detection by nanocoated fiber label-free biosensors. ACS Sens, 2018, 3: 936–943
41 Zhou W J, Mandia D J, Barry S T, et al. Absolute near-infrared refractometry with a calibrated tilted fiber Bragg grating. Opt Lett, 2015, 40: 1713
42 Guo T, Liu F, Liu Y, et al. In-situ detection of density alteration in non-physiological cells with polarimetric tilted fiber grating sensors. Biosens Bioelectron, 2014, 55: 452–458
43 Sutapun B, Tabib-Azar M, Kazemi A. Pd-coated elastooptic fiber optic Bragg grating sensors for multiplexed hydrogen sensing. Sens Actuat B-Chem, 1999, 60: 27–34
44 Allison E G, Bond G C. The structure and catalytic properties of palladium-silver and palladium-gold alloys. Catal Rev, 1972, 7: 233–289
45 Liu Y K, Liang B H, Zhang X J, et al. Plasmonic fiber-optic photothermal anemometers with carbon nanotube coatings. J Lightwave Technol, 2019, 37: 3373–3380
46 Lao J J, Sun P, Liu F, et al. In situ plasmonic optical fiber detection of the state of charge of supercapacitors for renewable energy storage. Light Sci Appl, 2018, 7: 34